0026-895X/06/7005-1542–1554$20.00
MOLECULAR PHARMACOLOGY
Copyright © 2006 The American Society for Pharmacology and Experimental Therapeutics
Mol Pharmacol 70:1542–1554, 2006

Vol. 70, No. 5
26187/3146143
Printed in U.S.A.

The Concerted Contribution of the S4–S5 Linker and the S6 Segment to the Modulation of a K_v Channel by 1-Alkanols

Aditya Bhattacharji, Benjamin Kaplan, Thanawath Harris, Xiaoguang Qu, Markus W. Germann, and Manuel Covarrubias

Department of Pathology, Anatomy and Cell Biology, Jefferson Medical College of Thomas Jefferson University, Philadelphia, Pennsylvania (A.B., B.K., T.H., M.C.); and Department of Chemistry, Georgia State University, Atlanta, Georgia (X.Q., M.W.G.)

Received May 1, 2006; accepted August 3, 2006

ABSTRACT

Gating of voltage-gated K^+ channels (K_v channels) depends on the electromechanical coupling between the voltage sensor and activation gate. The main activation gate of K_v channels involves the COOH-terminal section of the S6 segment (S6-b) and the S4–S5 linker at the intracellular mouth of the pore. In this study, we have expanded our earlier work to probe the concerted contribution of these regions to the putative amphipathic 1-alkanol site in the Shaw2 K^+ channel. In the S4–S5 linker, we found a direct energetic correlation between α-helical propensity and the inhibition of the Shaw2 channel by 1-butanol. Spectroscopic structural analyses of the S4–S5 linker supported this correlation. Furthermore, the analysis of chimeric Shaw2 and $K_v3.4$ channels that exchanged their corresponding S4–S5 linkers showed that the potentiation induced by 1-butanol depends on the combination of a single mutation in the S6 PVPV motif (PVAV) and the presence of the Shaw2 S4–S5 linker. Then, using tandem-heterodimer subunits, we determined that this potentiation also depends on the number of S4–S5 linkers and PVAV mutations in the K_v channel tetramer. Consistent with the critical contribution of the Shaw2 S4–S5 linker, the equivalent PVAV mutation in certain mammalian K_v channels with divergent S4–S5 linkers conferred weak potentiation by 1-butanol. Overall, these results suggest that 1-alkanol action in Shaw2 channels depends on interactions involving the S4–S5 linker and the S6-b segment. Therefore, we propose that amphiphilic general anesthetic agents such as 1-alkanols may modulate gating of the Shaw2 K^+ channel by an interaction with its activation gate.

The molecular basis of alcohol and general anesthetic action on neuronal ion channels has been investigated intensely in the past decade (Peoples et al., 1996; Diamond and Gordon, 1997; Harris, 1999; Campagna et al., 2003; Hemmings et al., 2005). The focus of these investigations is on determining the exact location of the sites, the molecular interactions involved, and the mechanisms responsible for the functional modulation of ion channels by 1-alkanols and other general anesthetic agents. The voltage-gated Shaw2 K^+ channel present in the nervous system of *Drosophila melanogaster* is inhibited by clinically relevant doses of 1-alkanols and inhaled anesthetics in a saturable fashion (Covarrubias et al., 1995; Hodge et al., 2005) (A. Bhattacharji and M. Covarrubias, unpublished data); this modulation involves the 13-amino acid amphipathic S4–S5 linker (Fig. 1), which may contribute to the 1-alkanol binding site in the channel (Harris et al., 2000; Shahidullah et al., 2003). In addition, substitution of alanine for a proline at the third position of the highly conserved PxPx motif (PVAV) in the S6 segment of the Shaw2 subunit converts the modulation by 1-alkanols from inhibition to potentiation (Harris et al., 2003). The recently published crystal structure of a mammalian voltage-gated K^+ channel (K_v channel) in the open state confirmed that this motif introduces a kink in the S6-b segment, which favors a direct interaction with the S4–S5 linker (Long et al., 2005) (Fig. 1). It has therefore been inferred that this interaction may be necessary for the opening of the internal S6 gate (inner helix bundle) through the electromechanical coupling between the voltage-sensing domain and the pore domain upon voltage-dependent activation of the K_v channel (Lu et al., 2002; Yifrach and MacKinnon, 2002; Long et al., 2005; Ferrer et al., 2006). The basic operation of Shaw2 K^+ channels is likely to be similar, because they are highly homologous to other eukaryotic K_v channels (Salkoff et al., 1992).

To gain further insights into the mechanisms and struc-

This work was supported by National Institutes of Health research grant R01-AA010615 (to M.C.).
A.B. and B.K. contributed equally to this study.
Article, publication date, and citation information can be found at http://molpharm.aspetjournals.org.
doi:10.1124/mol.106.026187.

ABBREVIATIONS: K_v, voltage-gated K^+ channel; 1-BuOH, 1-butanol; G_p-V, peak chord conductance-voltage; TFE, 2,2,2-trifluoroethanol; NOESY, nuclear Overhauser effect spectroscopy.

tural basis of the inhibition of Shaw2 K^+ channels by 1-alkanols, we investigated the energetic relationship between the apparent binding of 1-BuOH to the channels and the α-helical propensity of the S4–S5 linker and verified the secondary structural features of distinct S4–S5 linkers by CD and NMR spectroscopy. Then, we hypothesized that both inhibition and potentiation of Shaw2 channels by 1-alkanols may occur by interactions with structural components of the channel's activation gate; thus, we sought to determine whether the Shaw2 S4–S5 linker may also contribute to the potentiation of the PVAV mutants by 1-BuOH, and whether a full complement of Shaw2 S4–S5 linkers and PVAV mutations in a channel tetramer was necessary to support the potentiation. Finally, we sought to determine whether the PVAV mutation, which is expected to disrupt gating, might also confer potentiation by 1-BuOH in mammalian K_v channels with divergent S4–S5 linkers, and we evaluated the effect of the PxAx mutation on voltage-dependent gating of nine distinct K_v channels, including various hybrid and chimeric channels. These studies helped us to determine the extent to which the S4–S5 linker and the S6-b segment might act in concert to confer the modulation of the Shaw2 K^+ channel by 1-alkanols and led us to suggest a working model of the Shaw2 1-alkanol site involving components of the activation gate (Covarrubias et al., 2005). Furthermore, across different K_v channel subfamilies, we have confirmed the crucial role of the PxPx motif in coupled voltage-dependent gating.

Materials and Methods

Materials and Reagents. The Shaw2 and K_v channel cDNAs were maintained as reported previously (Covarrubias et al., 1995; Jerng et al., 1999; Beck and Covarrubias, 2001). The rat $K_v2.1$ cDNA was a gift from Dr. Martin Stocker (University College London). The Shaw2-$K_v3.4$ tandem heterodimer was created by Dr. Aguan Wei (Washington University, St. Louis, MO) as described previously (Covarrubias et al., 1995). The Δ28-$K_v3.4$ mutant lacks the first 28 amino acids, which constitute the inactivation domain of this channel (Covarrubias et al., 1994). The QuikChange site-directed mutagenesis kit (Stratagene, La Jolla, CA) was used to create all mutations. The mutations were verified by automated DNA sequencing (Kimmel Cancer Center, Thomas Jefferson University). For expression in *Xenopus laevis* oocytes, mRNA was synthesized in vitro as described previously (Harris et al., 2000, 2003). 1-BuOH is high-performance liquid chromatography-grade and was purchased from Fisher Scientific (Hampton, NH). To harvest oocytes, *X. laevis* frogs were handled according to a protocol approved by the IACUC of Thomas Jefferson University.

Electrophysiology. Two to 5 days after the injection of the mRNA into defolliculated oocytes, the two-electrode voltage-clamp method was used to record the expressed whole-oocyte currents in normal extracellular bath solution (ND96) according to established procedures (Covarrubias et al., 1995; Jerng et al., 1999; Harris et al.,

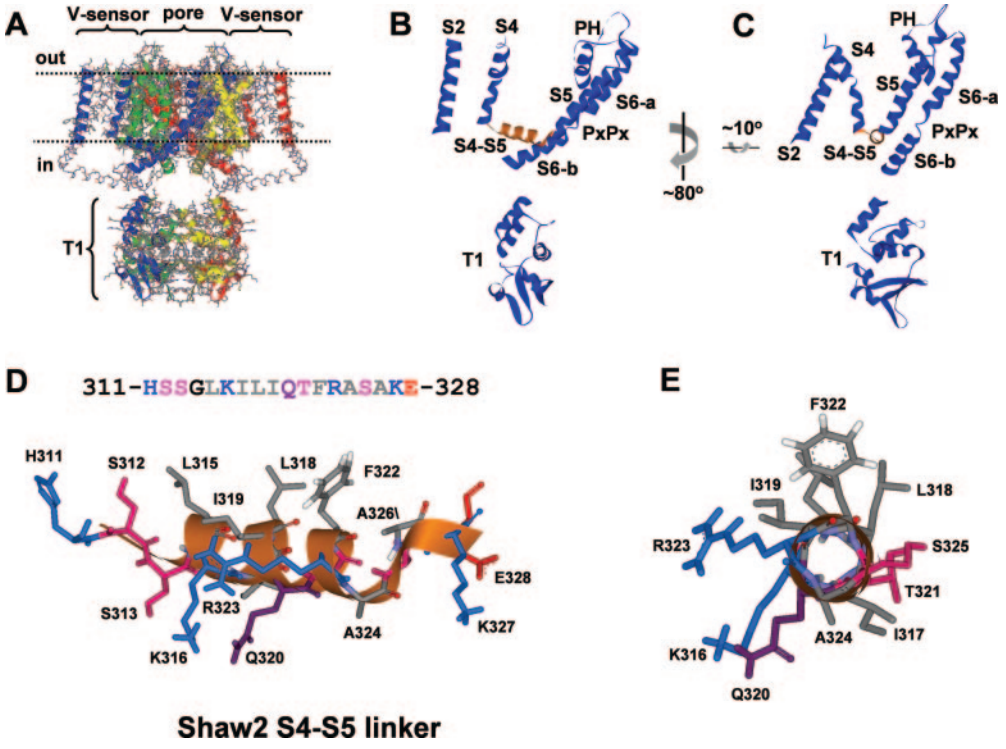

Fig. 1. Structural model of a K_v channel and the Shaw2 S4–S5 linker. A, functional domains of the K_v channel in the open state. The pore domain includes the selectivity filter, and the voltage sensing domain includes the S4 voltage sensor. The coordinates of the $rK_v1.2$ crystal structure were used to build this model (Long et al., 2005). Each color of the model corresponds to a subunit of the tetrameric channel structure. B, a subunit of the K_v channel. Only the blue subunit from A is shown. The S1–S4 segments constitute the voltage sensing domain (S2 and S4 are shown); the S5, PH, and S6 segments constitute the pore domain (PH is the pore helix in the selectivity filter). Note that the intracellular S4–S5 linker highlighted in orange connects the voltage sensing and pore domains. C, homology model of the Shaw2 S4–S5 linker. The amino acid sequence above the model includes the S4–S5 linker (the α-helix between Ser312 and Ala326). The S4–S5 linker of the $rK_v1.2$ was used as the parent structure. Amino acid side chains are color coded according to charge and polarity (gray, nonpolar; pink, polar; purple, polar; red, negatively charged; blue, positively charged). D, view of the S4–S5 linker from the COOH side of the α-helix. Note the amphipathic character of segment: positively charged residues face the aqueous environment, whereas the nonpolar residues and two polar residues (Thr321 and Ser325) face the membrane or the channel protein. The side chains of Thr321 and Ser325 are expected to face the hydrophobic S6-b segment. The features of this interface suggest the presence of an amphipathic site that may accommodate 1-alkanols (Shahidullah et al., 2003; Covarrubias et al., 2005).

2000, 2003). In general, macroscopic currents were low-pass-filtered at 0.5 to 1 kHz and digitized at 1 to 2 kHz. The program pClamp 8–9 (Molecular Devices, Sunnyvale, CA) was used for acquisition, data reduction and initial analysis. Leak current was subtracted off-line by assuming a linear leak. The peak chord conductance-voltage relations (G_p-V relations) were plotted to evaluate the voltage dependence of the channels. G_p was calculated as follows: $G_p = I_p/(V_c - V_r)$, where I_p is the peak current, V_c is the command voltage, and V_r is the reversal potential under normal ionic conditions (−90 to −95 mV in 2 mM external K^+). When currents exhibited very slow activation and no apparent inactivation, an estimation of the peak current was obtained from the maximal current at the end of a long step depolarization (1500–3000 ms). To approximate the empirical activation parameters of the channels ($V_{1/2}$ and Z; Table 2), the G_p-V relations were described by assuming first- or fourth-order Boltzmann distributions (Smith-Maxwell et al., 1998). All G_p-V relations were normalized to the estimated G_{max}. In general, first-order Boltzmann distributions did not describe the G_p-V relations adequately. When the voltage dependence of the mutant currents became rightward-shifted or when there was evidence of rectification caused by Mg^{2+} blockage of K_v3.4 channels at high voltages (Rettig et al., 1992), the Boltzmann distributions accounted only for part of the G_p-V relation. The midpoint voltage of the G_p-V curves ($V_{1/2}$) described by a fourth-order Boltzmann function, was calculated as follows: $V_{1/2} = V_a - 1.67k$, where V_a is the midpoint voltage for activation of one subunit and k is the slope factor (Smith-Maxwell et al., 1998). All recordings were obtained at 23 ± 1°C.

CD Spectroscopy. Peptides corresponding to the S4–S5 linkers of Shaw2 and K_v3.4 were synthesized as described previously (Shahidullah et al., 2003). The peptides were dissolved in 5 mM phosphate buffer, pH 6.0, at a final concentration of 50 μM. To promote the α-helical structure of the peptides, TFE was added to the solutions. A spectropolarimeter (J710; Jasco, Tokyo, Japan) was used to obtain all CD spectra at room temperature. Each spectrum was the average of four scans. The resulting spectra were analyzed and deconvoluted using the CDPro software package (Sreerama and Woody, 2000, 2004; Sreerama et al., 2000).

NMR Spectroscopy. Synthetic peptides were dissolved in buffer containing: 10 mM sodium phosphate, 0.1 mM EDTA, and 0.011 mM 2,2-dimethyl-2-silapentane-5-sulfonate sodium salt. A 600-MHz spectrophotometer (Avance; Bruker, Newark, DE) was used to conduct NMR experiments at different temperatures. One-dimensional spectra were collected using presaturation and jump-and-return pulse sequences to suppress the solvent signal. At the peptide concentrations required for the NMR analysis (1 mM), the Shaw2 peptide was soluble at pH <4.5. Therefore, for a direct comparison of the two peptides, the collection of one-dimensional NMR spectra was carried out at pH 4.2 and a temperature of 288 K. For two-dimensional spectra, the mixing times were 75 and 400 ms for total correlation spectroscopy (2000 × 512, 32 scans) and nuclear Overhauser effect spectroscopy (NOESY; 2000 × 512, eight scans), respectively. NMR spectra were assigned using Sparky (http://www.cgl.ucsf.edu/home/sparky/) following standard methods (Wüthrich, 1986).

Calculations. Curve fitting and data display and analysis were carried out in Origin 7.5 (OriginLab Corp., Northampton, MA) or Sigmaplot 9.0 (Systat Software Inc., Point Richmond, CA). Dose-response curves were analyzed as described previously (Covarrubias et al., 1995; Harris et al., 2000; Shahidullah et al., 2003). In brief, the normalized equilibrium dose-inhibition curves were empirically described by assuming the Hill equation: $I/I_{max} = 1/[1 + (A/K_{1/2})^{nH}]$, where A is the 1-BuOH concentration, $K_{1/2}$ is the drug concentration that induces 50% inhibition and n_H is the index of cooperativity or Hill coefficient. The Gibbs free energy change for apparent binding was calculated as follows: $\Delta G_B = RT \ln K_{1/2}$, where R is the ideal gas constant and T is absolute temperature.

Ideally, $K_{1/2}$ in the Hill equation is operationally related to the apparent dissociation constant by this relationship: $K_d = (K_{1/2})^n$, where n is the total number of binding sites per channel (Cantor and Schimmel, 1980). Given that various wild-type and mutant K_v channels exposed to various 1-alkanols yield $n_H \geq 1$ generally (Covarrubias et al., 1995; Harris et al., 2000; Shahidullah et al., 2003) and that K_v channels are tetrameric (Long et al., 2005), four interacting sites per channel ($n = 4$) are assumed implicitly throughout this empirical analysis (i.e., the channels may exhibit various degrees of relatively weak apparent positive cooperativity). The $\Delta\Delta G_B$ induced by a mutation was calculated relative to the corresponding wild type as explained in Fig. 2 legend. The assumed n is a scaling factor in the calculation of ΔG_B above; therefore, it does not affect the apparent $\Delta\Delta G_H - \Delta\Delta G_B$ correlation in Fig. 2B. In light of the empirical nature of this analysis, no model-dependent assumptions were made with respect to the mechanism of an apparent positive cooperativity.

According to algorithms developed by the Serrano laboratory (EMBL, Heidelberg, Germany) (Munoz and Serrano, 1994; Lacroix et al., 1998), the program AGADIR (http://www.embl-heidelberg.de/Services/serrano/agadir/agadir-start.html) was used to calculate the Gibbs free energy changes of the random-coil to α-helix equilibrium (ΔG_H) for the S4–S5 linker sequences examined in Fig. 2B. All results are expressed as the mean ± S.E. of n independent determinations. The Student's t test was used to evaluate the differences between mean values.

Experimental Limitations. To evaluate activation gating of the PVAV mutants, we plotted the G_p-V relation and assumed Boltzmann functions to describe and normalize the curve (as explained above). Given that some wild-type and mutant K_v channels exhibited dramatically different current kinetics and voltage dependence, more quantitative alternative approaches could not be applied for comparative purposes: the presence of voltage-dependent current kinetics and rapid inactivation impeded a reliable application of normalized tail current-voltage relations to determine steady-state activation parameters. In addition, under two-electrode voltage-clamp conditions, *X. laevis* oocytes do not tolerate the large membrane depolarizations (+80 to +200 mV) that would have been necessary to examine more complete G_p-V relations of mutants with severely depolarized voltage dependence. Despite these limitations, our analysis of G_p-V relations allowed an overall semiquantitative comparison of voltage-dependent gating and the relative shifts induced by the mutations in various K_v channels.

The measurement of complete 1-BuOH dose-potentiation relations for all K_v channels and their corresponding PVAV mutants was not practical. Relative to Shaw2 channels, the observed 1-BuOH sensitivities of other homomeric K_v channels were very low; at best, in one instance only, it was one third (~30%) of the Shaw2-P410A response at 15 mM 1-BuOH (100%). Moreover, as described previously (Harris et al., 2003), even the dramatic dose-dependent potentiation of the Shaw2-P410A channel at equilibrium exhibits no evident saturation at concentrations as high as 100 mM 1-BuOH. Therefore, for comparative purposes, we opted to evaluate the sensitivity of all K_v channels at a concentration of 1-BuOH that doubles the total Shaw2-P410A current at equilibrium (15 mM).

Results

Energetics of the S4–S5 α-Helicity and the Apparent Binding of 1-BuOH to the Shaw2 Channel. The K_v3.4 channel is normally resistant to 1-alkanols (Covarrubias et al., 1995). It is noteworthy, however, that the progressive conversion of the K_v3.4 S4–S5 linker into that of Shaw2 and vice versa is associated with the progressive gain and loss of the inhibition of these channels by 1-BuOH, respectively (Harris et al., 2000). These results suggested that the structural effect of the mutations in the S4–S5 linker plays a significant role in determining the sensitivity of these K^+ channels to 1-alkanols. Thus, we have hypothesized that the α-helical propensity of the S4–S5 linker is critical to maintain the structural integrity of the putative 1-alkanol binding

site at the activation gate in the Shaw2 channel (Harris et al., 2000). Studies with intact K_v1 channels or the isolated S4–S5 linker have shown that this segment is likely to adopt an α-helical configuration (Ohlenschlager et al., 2002; Long et al., 2005). We found that a peptide corresponding to the S4–S5 linker of Shaw2 is more likely to adopt a defined secondary structure than that of $K_v3.4$ (Shahidullah et al., 2003). To test the hypothesis more rigorously, we investigated the energetic relationship between the apparent binding of 1-BuOH to the Shaw2 channel and the calculated α-helical propensity of the S4–S5 linker for various Shaw2 and $K_v3.4$ mutants with distinct sensitivities to 1-BuOH (*Materials and Methods*; Fig. 2A). For this experiment, several constructs were chosen to cover the range of α-helical propensities between the wild-type S4–S5 linkers of Shaw2 and $K_v3.4$. The equilibrium dose-inhibition relationships showed that the Shaw2 wild-type and the $K_v3.4$ chimera hosting the Shaw2 S4–S5 linker exhibited the lowest apparent dissociation constants and Hill coefficients only modestly above unity, and $K_v3.4$ wild-type and Shaw2 hosting the $K_v3.4$ S4–S5 exhibited the highest apparent dissociation constants and Hill coefficients significantly greater than unity. The dose-inhibition relations of mutants with partial conversion in the S4–S5 linker exhibited intermediate features. Supporting the hypothesis, we found that, for the wild-type and several mutant channels, the 1-BuOH binding free energy change was directly correlated with the free energy change of the random-coil to α-helix equilibrium calculated for segments of 19 residues encompassing the 13 critical amino acids in the S4–S5 linker (Fig. 2B). This result suggests that the interaction of 1-alkanols with Shaw2 channels may depend on the high α-helical propensity in the S4–S5 linker. In addition, this conclusion is supported by the results from the single $K_v3.4$-G371I mutant, which exhibited 1-alkanol interaction with intermediate energetic features (K3 in Fig. 2B) (Covarrubias et al., 1995), and CD spectroscopy demonstrated previously that the S4–S5 linker of this mutant has an intermediate α-helical propensity between that of the wild-type versions of Shaw2 and $K_v3.4$ (Shahidullah et al., 2003). These results were strengthened further by detailed structural analyses of the Shaw2 and $K_v3.4$ S4–S5 linkers, as described below.

Structural Analysis of the S4–S5 Linkers from Shaw2 and $K_v3.4$. As previously shown in the absence of TFE (see *Materials and Methods*) (Shahidullah et al., 2003), the CD spectra demonstrated that the Shaw2 S4–S5 linker peptide is

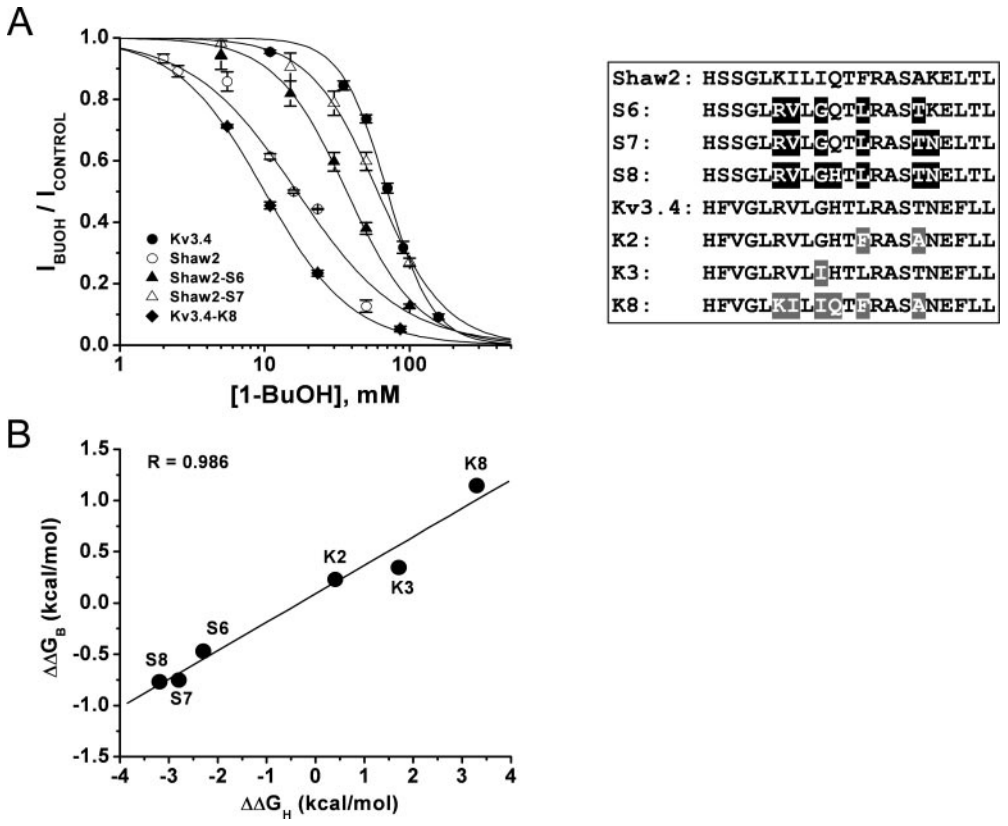

Fig. 2. The apparent binding affinity of the Shaw2 1-alkanol site and the α-helical propensity of the S4–S5 linker are strongly correlated. A, 1-BuOH equilibrium dose-inhibition curves for wild-type Shaw2 and wild-type $K_v3.4$, and various S4–S5 linker mutants of these channels (Shaw2 mutants, S6 and S7; $K_v3.4$ mutants, K8). The corresponding S4–S5 linker sequences are indicated in the inset. Complete dose-inhibition curves were obtained for the wild-type and mutant channels indicated in this inset. For clarity, only five selected curves are shown. The solid lines are the best-fit binding isotherms (*Materials and Methods*). B, correlation between the apparent Gibbs free energy change of 1-BuOH binding and the calculated Gibbs free energy change of the random-coil to α-helix equilibrium (Muñoz and Serrano, 1994; Lacroix et al., 1998) (Shaw mutants: S6, S7, and S8; $K_v3.4$ mutants: K2, K3, and K8). The solid line is the best-fit linear regression with the correlation coefficient indicated in the graph. The $\Delta\Delta G$ values are calculated relative to the corresponding wild-type as follows: $\Delta\Delta G_B = \Delta G_{B,WT} - \Delta G_{B,MUT}$; $\Delta\Delta G_H = \Delta G_{H,WT} - \Delta G_{H,MUT}$. $\Delta G_B = RT \ln K_{1/2}$ (*Materials and Methods*). The best-fit parameters were: Shaw2-WT: $K_{1/2} = 18.9 \pm 1.4$ mM, $n_H = 1.2 \pm 0.1$; S6: $K_{1/2} = 37 \pm 3.7$ mM, $n_H = 1.8 \pm 0.1$; S7: $K_{1/2} = 63.9 \pm 8.4$ mM, $n_H = 1.9 \pm 0.2$; S8, $K_{1/2} = 50$ mM, $n_H = 2$ (Harris et al., 2000); $K_v3.4$-WT: $K_{1/2} = 70$ mM, $n_H = 2.8$ (Harris et al., 2000); K2: $K_{1/2} = 48.5 \pm 1.2$ mM, $n_H = 1.7 \pm 0.1$; K3: $K_{1/2} = 39$ mM, $n_H = 1$ (Covarrubias et al., 1995); K8: $K_{1/2} = 10$ mM, $n_H = 1.4$ (Harris et al., 2000). ΔG_H was calculated as reported by Muñoz and Serrano (1994) and Lacroix et al. (1998).

partially structured and that of K_v3.4 is unstructured (Fig. 3). Because the concentration of TFE was increased from 0 to 85%, both peptides adopted an α-helical structure; however, the Shaw2 peptide seemed to require lower TFE concentrations (Fig. 3). These observations are in agreement with our previously reported results (Shahidullah et al., 2003). A closer examination of improved CD spectra revealed an isodichroic point in the profiles from the K_v3.4 S4–S5 linker peptide, which suggests a simple two-state transition from random-coil to α-helix (Fig. 3). In contrast, the structural transition of the Shaw2 S4–S5 linker does not involve a simple two-state transition because the CD spectra exhibited no isodichroic point (Fig. 3). Supporting this interpretation, the ellipticity at 220 nm is close to a plateau between 30 and 85% TFE, whereas the ellipticity at 208 nm continues to change. Deconvolution of the new CD spectra revealed the presence of a significant β-sheet structure in the Shaw2 peptide at 0% TFE (Table 1); as expected, the K_v3.4 peptide in the absence of TFE is mostly random-coil (Table 1). The Shaw2 peptide reached its maximum α-helical content as the TFE concentration increased from 50 to 85%, whereas the structural conversion of the K_v3.4 peptide to α-helix is more gradual (Fig. 3 and Table 1). The CD analyses of the S4–S5 linker peptides strongly suggest the presence of intrinsic structural differences between the S4–S5 linkers of Shaw2 and K_v3.4 channels.

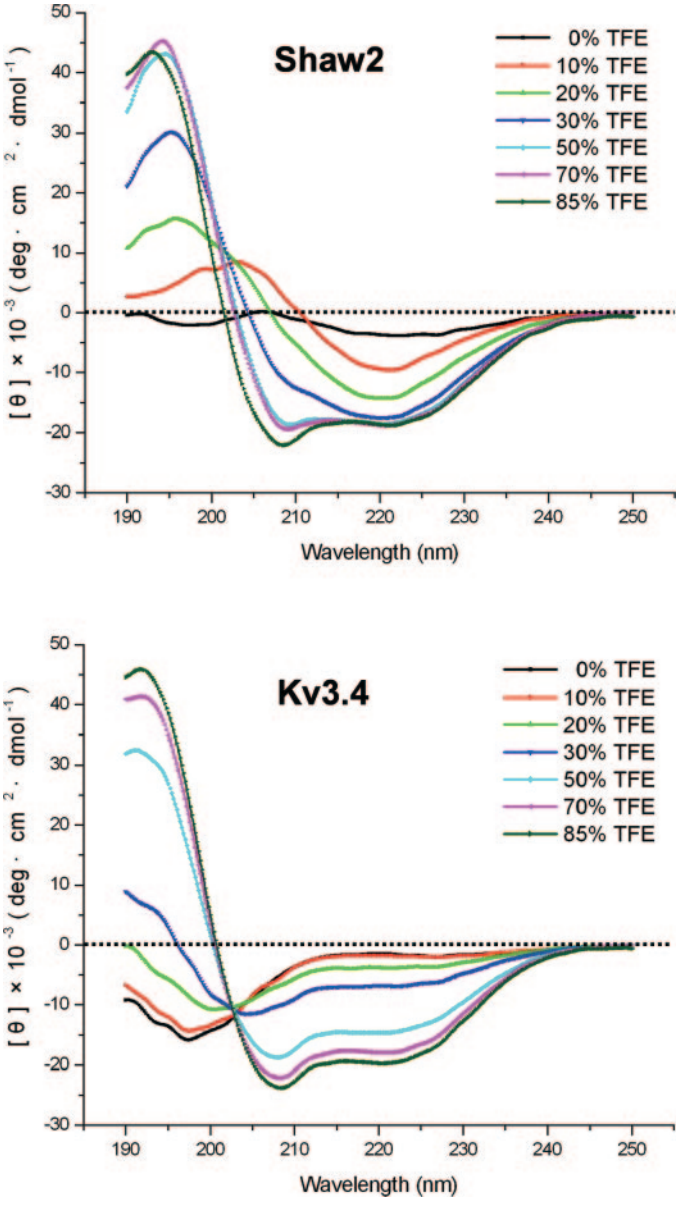

Fig. 3. CD spectra of Shaw2 (A) and K_v3.4 (B) S4–S5 linkers titrated from 0 to 85% TFE. CD spectra (four scans) of S4–S5 linkers of Shaw2 and K_v3.4 were recorded at room temperature in 2-mm cuvettes (*Materials and Methods*). The molar ellipticity [θ] is given on per-residue basis. To promote the α-helical structure of the peptides, both peptides were titrated with TFE from 0 to 85%. The deconvolutions of the titration curves at different TFE concentrations are shown in Table 1.

More conclusively, NMR spectroscopy revealed the structural differences between the Shaw2 and K_v3.4 linker peptides by examining the two-dimensional total correlation spectroscopy and NOESY spectra. Figure 4A shows the corresponding connectivities of the Shaw2 peptide in 0 and 50% TFE at a temperature of 288 K. At 0% TFE, the Shaw2 peptide (but not K_v3.4) exhibited weak NH-NH sequential connectivity, which is compatible with a β-sheet formation. At low TFE concentrations, this peptide contains both β-sheet and random-coil components; this is consistent with the absence of an isodichroic point in the Shaw2 CD spectra (Fig. 3B). At 50% TFE, the number of medium range connectivities is quite substantial and characteristic of an α-helical structure. Under the same conditions, the K_v3.4 peptide shows a different behavior (Fig. 4B). In particular, no characteristic long-range connectivities are observed, which originates from the lower amount of α-helix formation and the dynamic differences in the α-helix stability of the peptides. Thus, despite the necessary differences in the sample conditions of the two measurements (*Materials and Methods*), CD and NMR spectroscopy yielded compatible results, which suggests intrinsic structural differences between the Shaw2 and the K_v3.4 peptides. Overall, these structural analyses firmly confirm the greater α-helical propensity of the Shaw2 S4–S5 linker, and strongly support a relationship between the stability of the S4–S5 linker's secondary structure and the apparent affinity of the 1-alkanol site in Shaw2 and mutant K_v3.4 channels (Fig. 2).

The Potentiation of K_v Channels by 1-BuOH Depends on the Structure of the S4–S5 Linker. Recent reports have provided strong evidence to support the interaction between the S4–S5 linker and the S6-b segment in eukaryotic K_v channels as the basis of voltage-dependent activation gating (Lu et al., 2002; Tristani-Firouzi et al., 2002; Ding and Horn, 2003; Ferrer et al., 2006). Furthermore, the crystal structure of the K_v1.2 channel in the open state shows a direct physical interaction between these segments (Long et al., 2005) (Fig. 1). From our studies of the Shaw2 channel, we have suggested previously that the interface between the S4–S5 linker and the S6-b segment may constitute the amphipathic binding site for 1-alkanols (Harris et al., 2000, 2003; Shahidullah et al., 2003; Covarrubias et al., 2005). Therefore, we asked whether the greater α-helical propensity of the Shaw2 S4–S5 linker is also a structural feature that supports the potentiation of the PVAV Shaw2 mutant by 1-alkanols. A full complement of K_v3.4 S4–S5 linkers and PVAV mutations would suppress the potentiation of Shaw2 by 1-BuOH; conversely, a full complement of Shaw2 S4–S5 linkers and PVAV mutations would confer enhanced potentiation of K_v3.4 by 1-BuOH. It would seem

that the PVAV mutation alters the kink of the S6-b segment, which changes its relationship with the S4–S5 linker. To test these hypotheses, we examined the effect of PVAV mutations in a chimeric Shaw2 channel hosting the S4–S5 linker from K_v3.4 (Shaw2-SK chimera) and a chimeric K_v3.4 channel hosting the S4–S5 linker from Shaw2 (K_v3.4-KS chimera). Relative to the Shaw2 P410A, the Shaw2 SK-chimera-P410A exhibited a 5-fold reduction in the potentiation induced by 15 mM 1-BuOH (+18 ± 3%; Fig. 5); the K_v3.4 KS chimera-P469A was potentiated 2 to 3 times better (+65 ± 4%) than K_v3.4-P469A or Δ28-K_v3.4-P469A (Figs. 5 and 7). Although the presence of the Shaw2 S4–S5 linker in K_v3.4 did not fully recapitulate the largest response of the Shaw2-P410A, it is clear that the S4–S5 linker plays a substantial role as a determinant of the potentiation induced by 1-BuOH. Additional unexplored differences in the Shaw2 background may account for the larger potentiation of the Shaw2-P410A (Smith-Maxwell et al., 1998). We propose that both the inhibition and potentiation of Shaw2 channels by 1-alkanols depend mainly on the intrinsic secondary structural features of the S4–S5 linker (Harris et al., 2000, 2003; Shahidullah et al., 2003). The Shaw2 S4–S5 linker with a greater α-helical propensity supports greater inhibition and potentiation by 1-alkanols.

Two PVAV Mutations and Two Shaw2 S4–S5 Linkers in the K_v Channel Tetramer Are Sufficient to Confer Potentiation by 1-BuOH. In a tetrameric K_v channel, each S4–S5 linker is paired with an S6-b segment (Fig. 1). Would the modulation of a heterotetrameric K_v channel by 1-BuOH also depend on the number of Shaw2 subunits and PVAV mutations? Consistent with the presence of a heteromeric channel, we have shown previously that a recombinant K_v channel made of two K_v3.4-Shaw2 tail-to-head tandem heterodimers exhibits inactivation kinetics and inhibition by 1-alkanols that were intermediate between those of Shaw2 (1-alkanol-sensitive) and K_v3.4 1-alkanol-resistant) (Covarrubias et al., 1995). Therefore, we hypothesized that the potentiation of K_v3.4-Shaw2 PVAV mutants by 1-BuOH may also be a function of the total number of PVAV mutations in the S6 segments (two or four) and Shaw2 S4–S5 linkers. Figure 6, A–D, illustrates the schematic structures of the K_v3.4-Shaw2 dimer of dimers with no PVAV mutations, two PVAV mutations in either the Shaw2 or the K_v3.4 moieties, or four PVAV mutations in the hybrid tetramer. As shown before, the hybrid K_v3.4-Shaw2 channel exhibited slow inactivation kinetics that is intermediate between that of the K_v3.4 channel and the Shaw2 channel (Covarrubias et al., 1995) (Fig. 9). The PVAV mutations K_v3.4[P469A] or the Shaw2[P410A] slowed current kinetics dramatically; however, the effect of the K_v3.4[P469A] mutation was even more severe, and the double K_v3.4[P469A]-Shaw2[P410A] mutation induced no apparent further slowing (Fig. 9A). Exposure of the wild-type K_v3.4-Shaw2 hybrid channel to 15 mM 1-BuOH induced a modest inhibition of the outward current

TABLE 1
Calculated percentage of secondary structures in the Shaw2 and Kv3.4 S4-S5 linkers at different TFE concentrations
The CDPro package, including SELCON3, CDSSTR, and CONTINL routines, was used to deconvolve the CD spectra in Fig. 3. The data listed are the results from CONTINLL, which has the lowest root-mean-square deviation and normalized root-mean-square deviation values.

TFE	Shaw2				Kv3.4			
	α-Helix	β -Sheet	Turn	Random coil	α-Helix	β-Sheet	Turn	Random Coil
				%				
0%	4.8	29.8	27.9	37.4	2.3	10.3	5.8	81.6
50%	65	14.7	0	20.4	54	9.3	12.5	24.1
85%	71	9.3	4.1	15.7	68.4	8.1	4.5	19.1

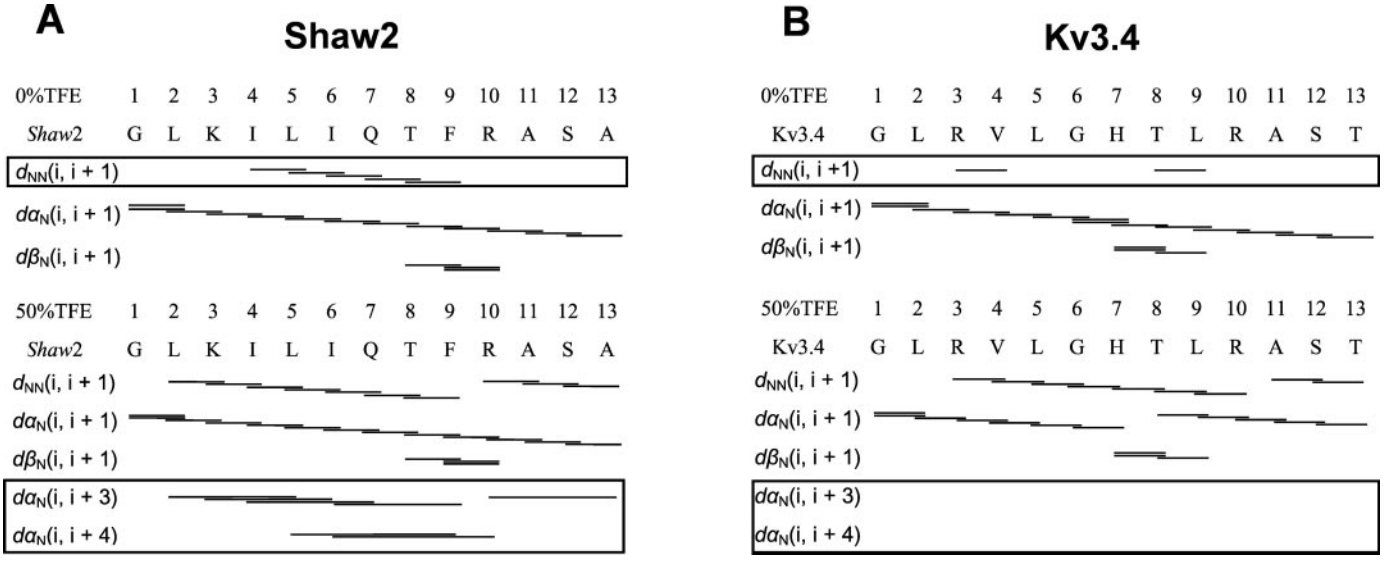

Fig. 4. NMR distance connectivities based on 400-ms NOESY spectra for Shaw2 and K_v3.4 S4–S5 linkers in the absence and presence of 50% TFE. NMR distance connectivities are based on 400-ms NOESY spectra recorded at 288 K. Different secondary structure results in characteristic connectivities of NH-NH and Hα-n_H protons. The lack of medium range connectivities of the K_v3.4 S4–S5 linker in both 0 and 50% TFE confirms its greater resistance to adopt an α-helical structure. In contrast, a substantial number of sequential and medium range connectivities confirm the greater α-helical propensity of the Shaw2 S4–S5 linker.

(−17.4 ± 3%; Fig. 6E), which is intermediate between the responses of homomeric K_v3.4 and Shaw2 (−4% and −47%, respectively) (Harris et al., 2000). The presence of the PVAV mutation in either the K_v3.4 or the Shaw2 moiety of the tandem heterodimer conferred modest potentiation by 15 mM 1-BuOH (+18 ± 5 to +26 ± 5%; Fig. 6E); the difference between the responses of channels with singly mutated heterodimers was not statistically significant ($p = 0.056$). It is noteworthy that the double K_v3.4[P469A]-Shaw2[P410A] mutation enhanced the response by >2-fold (+55 ± 16%; $p < 0.01$) (Fig. 6E) but did not recapitulate the larger response of the Shaw2-P410A (~100% potentiation; Fig. 5). This result agrees with the chimera observations described above (Fig. 5) because even though all four PVPV kinks are disrupted in this hybrid channel, there are only two Shaw2 S4–S5 linkers. All together, these results show that mutational perturbation of two PVPV kinks (most likely on opposite sides of the tetramer) is sufficient to induce potentiation by 1-BuOH and that a full complement of PVAV mutations is necessary to support the maximal response. However, this maximal potentiation of the heterotetrameric K_v channel is limited by the absence of a full complement of Shaw2 S4–S5 linkers.

The S6 PxAx Mutation in Mammalian K_v Channels Confers Weak Potentiation by 1-BuOH. Exposing *X. laevis* oocytes expressing wild-type Shaw2 or Shaw2-P410A channels to 15 mM 1-BuOH induced ~50% inhibition or ~100% potentiation of the outward currents evoked by membrane depolarization, respectively (Harris et al., 2000, 2003) (Fig. 7). As shown before (Harris et al., 2000) and further demonstrated here, the structural features of the Shaw2 S4–S5 linker confer these robust responses. Given that the PxPx motif is highly conserved in Shaker-related K_v channels and that the S4–S5 linkers are more divergent, we sought to determine whether the PxAx mutation would be sufficient to confer potentiation induced by 1-BuOH in mammalian K_v channels. Among representative wild-type members of the four subfamilies of Shaker-related K_v channels, K_v4.3 was the most sensitive (−15 ± 7%), and the others (K_v1.4, K_v2.1, K_v3.4, Δ28-K_v3.4) exhibited little or no response to 1-BuOH (Fig. 7). These results confirmed earlier observations showing that most K_v channels are relatively resistant to 1-alkanols (Anantharam et al., 1992). Therefore, we hypothesized that without the structural features of the Shaw2 S4–S5 linker, the PxAx mutation in mammalian K_v

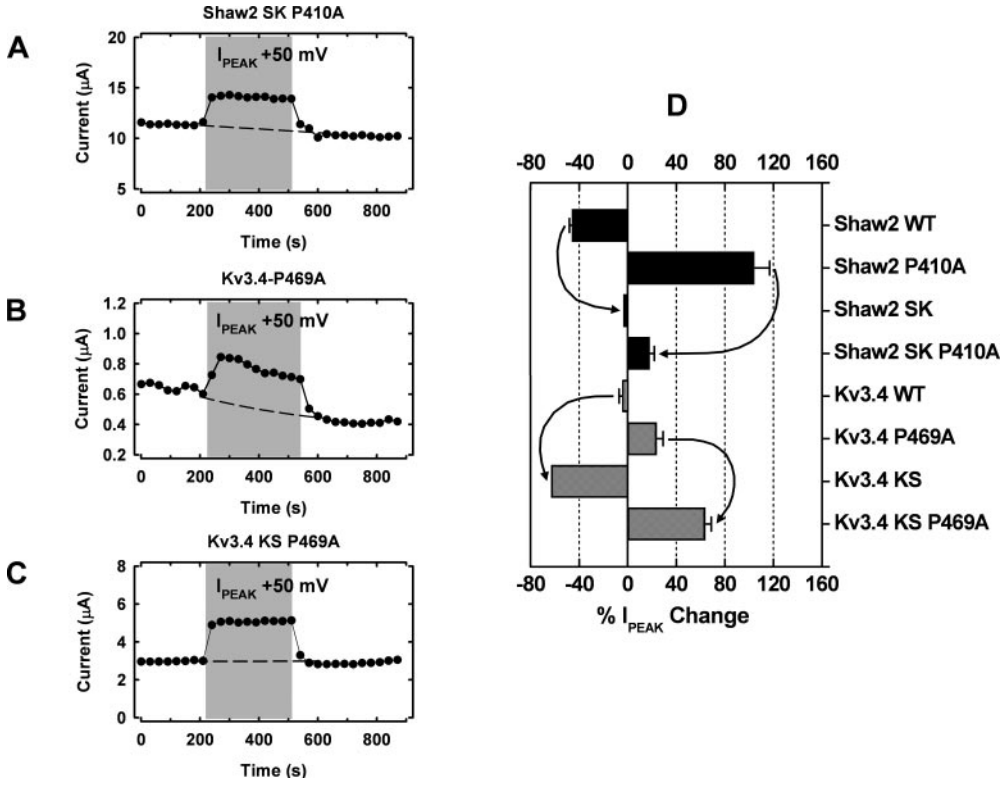

Fig. 5. The role of the S4–S5 linker on the 1-BuOH modulation of Shaw2 and K_v3.4 in the absence and presence of the PVAV mutation in the S6 segment. A–C, representative time courses of peak currents (I_{PEAK}) recorded at 30-s intervals. The channels tested are indicated in the figure. The outward currents were evoked by a step depolarization from −100 to + 50 mV. The shaded region of the time courses indicates the exposure time to 15 mM 1-BuOH. The I_{PEAK} run-down results from cumulative inactivation (except in C, which has no run-down). Thus, to calculate the change in the I_{PEAK} level, 7 to 10 points of the time courses before 1-BuOH and after washout were used to fit the following function (exponential plus sloping baseline): $y = A\exp(x/\tau) + mx + c$, where A is the amplitude of the exponential term, τ is the time constant, m is the slope, and c is a constant. Then, to estimate the I_{PEAK} change induced by 1-BuOH, the projected time course of run-down (dashed line) was used as the control I_{PEAK} value at the corresponding times. The % I_{PEAK} change was calculated from this formula: $((I_{PEAK,1\text{-}BuOH}/I_{PEAK,\ Control}) - 1) \times 100$. B, summary bar graph of the effect of 1-BuOH on I_{PEAK} (black bars: Shaw2 channels; patterned bars: K_v3.4 channels). For direct comparison, the data from Shaw2 WT, Shaw2 P410A, Shaw2 SK, and K_v3.4 KS are re-plotted from previously published studies (Harris et al., 2000, 2003). For Shaw2 SK-P410A, K_v3.4, K_v3.4-P469A, and K_v3.4 KS-P469A, $n = 4, 5, 5$, and 4, respectively. The difference between the values from K_v3.4 KS-P469A and those from the double-mutant tandem construct (Fig. 6) was not statistically significant ($p = 0.3$); the values from K_v3.4 KS-P469A and those from K_v3.4-P469A were significantly different ($p < 0.01$). The arrows indicate direction of the change induced by S4–S5 linker swapping (SK and KS in Shaw2 and K_v3.4, respectively) and the combination of PVAV mutations and linker swapping. Although the K_v3.4 S4–S5 linker in Shaw2 (SK) reduces both inhibition and potentiation, the Shaw2 S4–S5 linker in K_v3.4 (KS) increases both inhibition and potentiation.

channels may not confer a 1-BuOH response that matches that of the Shaw2-P410A mutant; nevertheless, we may observe weak and variable potentiation by 1-BuOH. The currents induced by the K_v1.4-P557A and Δ28-K_v3.4-P469A mutants were significantly potentiated by 15 mM 1-BuOH (+25 ± 3 and +19 ± 3%, respectively; Fig. 7). The 1-BuOH response of Δ28-K_v3.4-P469A was not dependent on the first 28 amino acids (inactivation domain) because the full-length K_v3.4-P469A was also potentiated by 1-BuOH, but its response seemed larger (+34 ± 5%; Fig. 7; $p = 0.02$). Although these responses were significant, they represent only a third to a fifth of the Shaw2-P410A response. The K_v2.1-P410A and K_v4.3-P400A mutants were almost completely insensitive to 1-BuOH. It seems that the effect of the PxAx mutation on K_v2.1 and K_v4.3 was to cancel their slight inhibition by 1-BuOH, from −6 ± 2 to +4 ± 2%, and from −15 ± 7 to +0.3 ± 5%, respectively. In agreement with the tandem-heterodimer observations (Fig. 6), these results demonstrate that the PxAx mutation is sufficient to confer weak potentiation by 1-BuOH in two distinct mammalian K_v channels (K_v1.4 and K_v3.4). However, the divergent S4–S5 linkers of these mutant channels cannot support a larger response comparable with that of the Shaw2-P410A channel.

The PxAx Mutations Impair Voltage-Dependence and Kinetics of K_v Channels in Distinct Subfamilies. The highly conserved PxPx motif in the S6 segment of K_v1 channels has received significant attention because the kink that it introduces seems to be critical for the coupling of the activation gate to the voltage sensor (del Camino and Yellen, 2001; Labro et al., 2003; Webster et al., 2004; Long et al., 2005). However, the contribution of the PxPx motif to activation and inactivation gating of other Shaker-related K_v subfamilies has not been investigated. Furthermore, in the context of this study, we attempted to learn whether the PxAx mutation may induce correlated effects on K_v channel gating and the 1-BuOH response. All mutant subunits produced functional channels, and the resulting currents exhibited profoundly altered kinetics and voltage dependence (Fig. 8; Table 2). Compared with their rapidly activating and inactivating wild-type counterparts, the K_v1.4-P557A and K_v4.3-P400A currents displayed slower activation and inactivation; the slowly inactivating K_v2.1-P410A and Δ28-K_v3.4-P469A currents displayed very slow activation (Fig. 8). The mutations also induced apparent depolarized shifts in the G_p-V relations, which ranged between +10 mV (K_v2.1-P410A) and +95 mV (K_v1.4-P557A) (Fig. 8, Table 2). In three cases (K_v3.4-P469A, Δ28-K_v3.4-P469A, and K_v4.3-P400A), the shifts were accompanied by a reduced apparent gating charge (Fig. 5; Table 2). Likewise, two or four PVAV mutations in hybrid K_v3.4-Shaw2 channels induced slower current kinetics and depolarized voltage dependence (Fig. 9, A and B). It is interesting, however, that the K_v3.4 P469A-Shaw2 mutant displayed a depolarized shift in the G_p-V relation that was larger than that of the K_v3.4-Shaw2 P410A

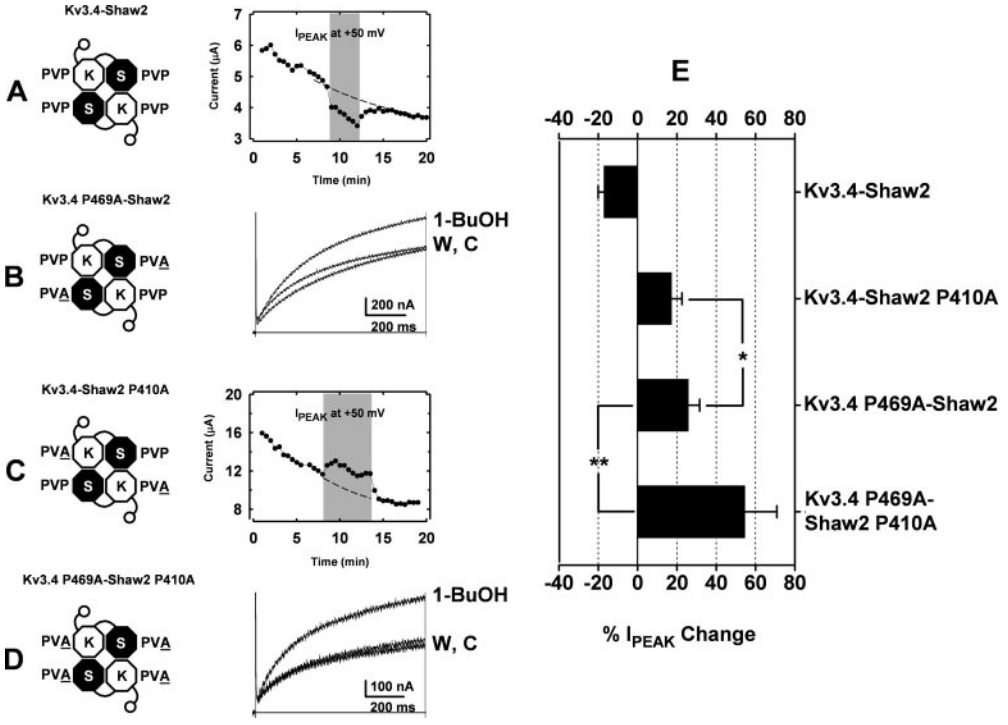

Fig. 6. The effect of PVAV mutations on the 1-BuOH modulation of K_v3.4-Shaw2 hybrid channels made of tandem heterodimer subunits. A. Cartoon representation of the K_v3.4-Shaw2 hybrid channel and time course of the peak current (I_{PEAK}) recorded and analyzed as explained in Fig. 5 legend. As described previously, the K_v3.4-Shaw2 heterodimer subunit was created as a tail-to-head tandem construct (Covarrubias et al., 1995). The NH_2-terminal inactivation domain of the K_v3.4 moiety represented as a small ball attached to the pore-forming subunit. Cartoon representations of the mutant hybrid channels with PVA mutations in different moieties (K_v3.4 = K; Shaw2 = S) or both moieties are also shown on the left of B to D. B, whole-oocyte outward currents evoked by a step depolarization from −100 to +50 mV. From the same oocyte, the current was recorded under control conditions in normal bath solution (C) (*Materials and Methods*), after equilibration in the presence of 15 mM 1-BuOH dissolved in bath solution (1-BuOH) and after washout with normal bath solution (W). C and D, these experiments were conducted as explained for A and B, respectively. E, summary bar graph of the effect of 1-BuOH on the peak current (I_{PEAK}). The difference between the values from K_v3.4-Shaw2 P410A and K_v3.4 P469A-Shaw2 was not statistically significant at ($p = 0.056$). In contrast, the difference between the values from the double PVAV mutant and those from the single PVAV mutants were significant ($p < 0.01$). For K_v3.4-Shaw2 P410A, K_v3.4 P469A-Shaw2, and K_v3.4 P469A-Shaw2 P410A, $n = 4$, 4, and 4, respectively; for the previously studied wild-type hybrid, K_v3.4-Shaw2, $n = 2$ (in this case, error bar indicates range).

mutant; the channel with a full complement of PVAV mutations (K_v3.4 P469A-Shaw2 P410A) displayed the largest depolarized shift and apparent loss of voltage dependence (reduced *Z*; Fig. 9B, Table 2). A semiquantitative evaluation of the voltage dependence of some chimeric channels hosting PVAV mutations was more difficult because of their much depolarized activation (*Materials and Methods*). Nevertheless, it was clearly apparent that the PVAV mutations induced slower current kinetics, no inactivation and more depolarized voltage dependence (Fig. 9, E and F). An apparent

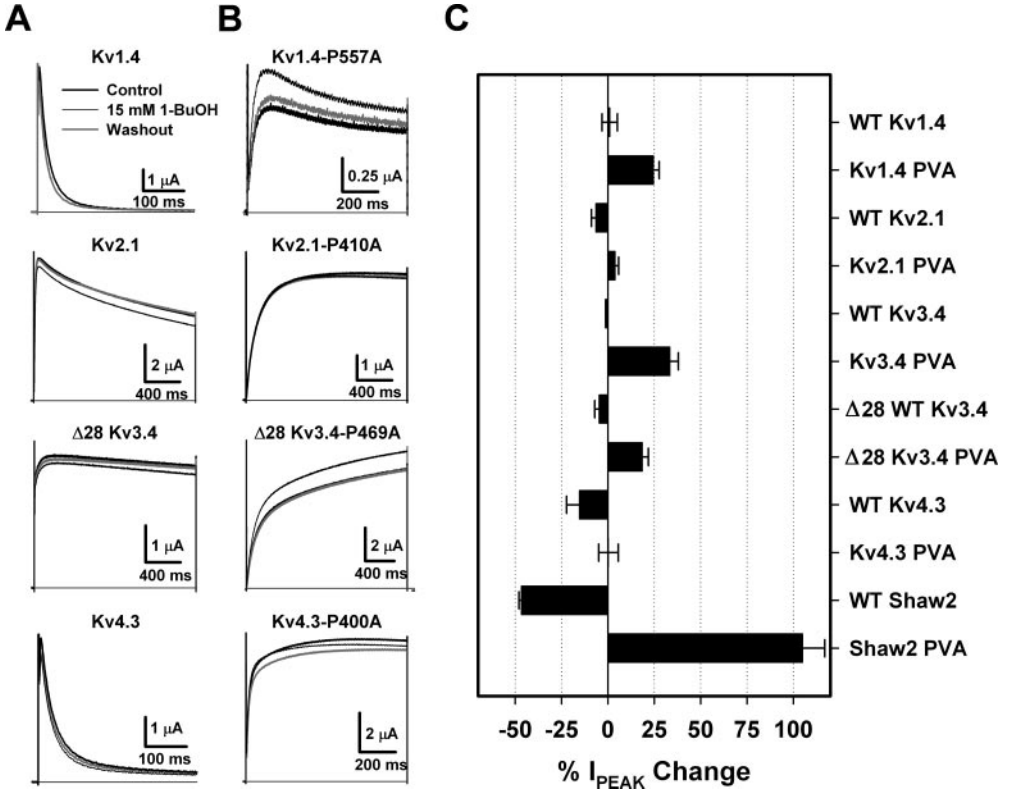

Fig. 7. Modulation of wild-type and PVAV mutant K_v channels by 1-BuOH. A and B, whole-oocyte outward currents evoked by a step depolarization from −100 to +50 mV. From the same oocyte, the current was recorded and analyzed as explained in legends for Figs. 5 and 6. The wild-type and mutant K_v channels exhibited no apparent run-down. C, summary bar graph of the effect of 1-BuOH on the peak current (I_{PEAK}). For direct comparison, the data from K_v3.4 WT, Shaw2 WT, and Shaw2-P410A are re-plotted from previously published studies (Harris et al., 2000, 2003). The % I_{PEAK} change was calculated as described in Fig. 5 legend. The values from K_v3.4-P469A and Δ28K_v3.4-P469A were significantly different (p = 0.02). For K_v1.4-WT, K_v1.4-PVA, K_v2.1-WT, K_v2.1-PVA, K_v3.4-PVA, Δ28 K_v3.4-WT, Δ28 K_v3.4-PVA, K_v4.3-WT, and K_v4.3-PVA, n = 5, 5, 6, 4, 3, 5, 5, 6, and 5, respectively.

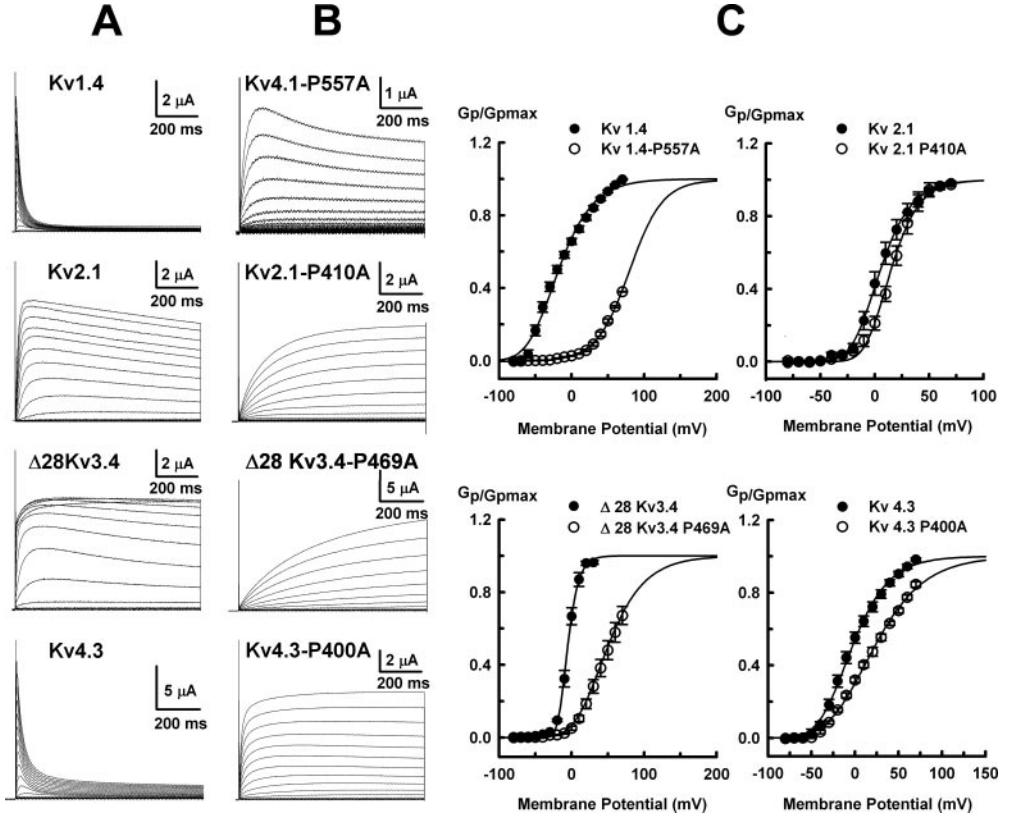

Fig. 8. Macroscopic kinetics and G_p-V relations of wild-type and mutant PxAx K_v channels. A, whole-oocyte outward currents evoked by step depolarizations from −100 mV to test voltages indicated in the graphs shown in C. The interpulse interval was ≥5 s. The longest interpulse interval was 30 s for K_v1.4 because it displayed very slow recovery from inactivation. B, whole-oocyte outward currents evoked as described in A for the corresponding PxAx mutants. C, chord peak conductance-voltage relations (see *Materials and Methods*) of the indicated wild-type K_v channels and their corresponding mutants. For all experiments, $n > 3$. The solid lines are the best-fit Boltzmann distributions (see *Materials and Methods*). The best-fit parameters are shown in Table 2.

exception was the Shaw2-SK P410A current, which displayed an instantaneous component followed by very slow activation and no apparent shift in the current-voltage relation (Fig. 9D). Overall, these results confirm the crucial role of the PxPx motif in K_v channel gating by demonstrating that the PxAx mutation exerts profound effects on current kinetics and voltage dependence of Shaker-related K_v channels in four distinct subfamilies.

The changes in the sensitivity of the channels to 1-alkanols were not always associated with major effects on electrophys-

TABLE 2

Analysis of Gp-V relations from wild-type and PxAx mutant Kv channels

Chord peak conductance-voltage relations were analyzed as described under *Materials and Methods*. Assuming Boltzmann distributions, the midpoint voltage $V_{1/2}$ and the slope factor k are the best-fit parameters that described these relations. The apparent gating charge Z was calculated as RT/kF, R is the gas constant, T is the absolute temperature, and F is the Faraday constant. $\Delta V_{1/2} = V_{1/2,MUT} - V_{1/2,WT}$. The wild-type and mutant tandem heterodimer subunits are as explained in Fig. 6. The $\Delta V_{1/2}$ values of the tandem heterodimer dimer PVAV mutants are relative to the $V_{1/2}$ of the tandem heterodimer composed of wild-type subunits.

Kv channel	$V_{1/2}$	Z	$\Delta V_{1/2}$	n
	mV	e_0	*mV*	
Kv1.4	−17.7 ± 2.4	0.87 ± 0.004	-	4
Kv1.4-P557A	+80	1.12 ± 0.05	+98	5
Kv2.1	+2.6 ± 3.8	1.62 ± 0.11	-	5
Kv2.1-P410A	+16.6 ± 3.4	1.47 ± 0.07	+14	4
Kv3.4	+7.1 ± 2.8	2.39 ± 0.04		3
Kv3.4-P469A	+82.6 ± 17.6	1.17 ± 0.19	+76	3
Δ28-Kv3.4	−5.2 ± 1.5	2.77 ± 0.15	-	4
Δ28-Kv3.4-P469A	+61.5 ± 11.1	0.78 ± 4.8	+67	6
Kv4.3	−6.5 ± 4.0	0.98 ± 0.02	-	5
Kv4.3-P400A	+22.4 ± 2.0	0.71 ± 0.01	+29	4
Kv3.4-Shaw2 Tandem	+12.2 ± 2.3	1.6 ± 0.06	-	4
Kv3.4-Shaw2[P410A]	+28.7 ± 3.6	1.26 ± 0.07	+16.5	3
Kv3.4[P469A]-Shaw2	+49 ± 2.2	0.88 ± 0.02	+36.8	3
Kv3.4[P469A]-Shaw2[P410A]	+76 ± 12	0.41 ± 0.04	+63.8	5

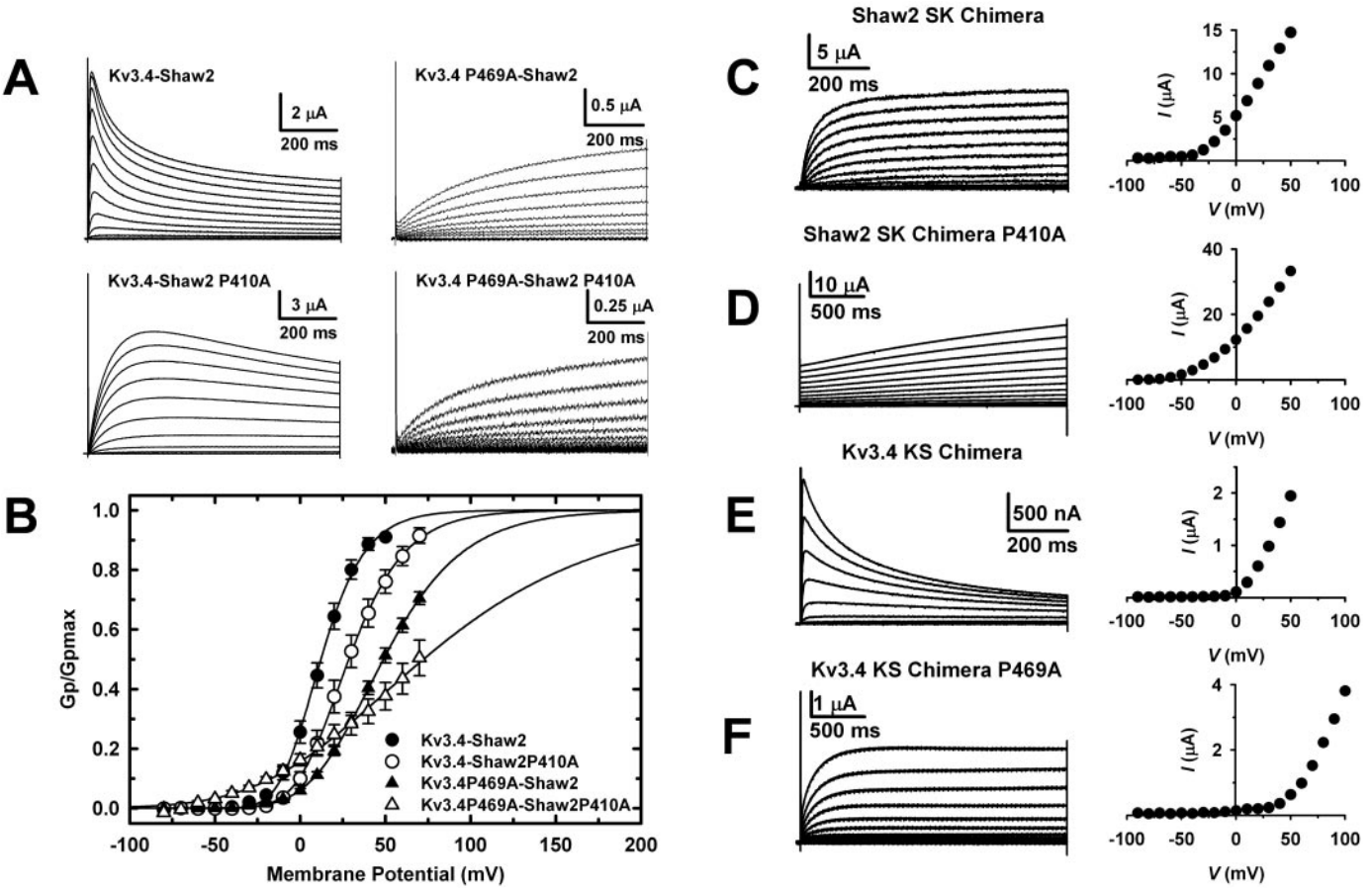

Fig. 9. Electrophysiological properties of K_v3.4-Shaw2 tandem heterodimer subunits and the effect of PVAV mutations. A, whole-oocyte outward currents evoked by step depolarization from −100 to test voltages indicated in the graphs shown in C. The interpulse interval was ≥5 s. The longest interpulse interval was 30 s for the K_v3.4-Shaw2 and K_v3.4-Shaw2 P410A hybrids because they displayed very slow recovery from inactivation. B, chord peak conductance-voltage relations (see *Materials and Methods*) of the hybrid K_v channel and the corresponding mutants. The solid lines are the best-fit Boltzmann distributions (see *Materials and Methods*). The best-fit parameters are shown in Table 2. C–F, whole-oocyte outward currents evoked by step depolarization from −100 mV to test voltages indicated in the current-voltage relations (right). The interpulse interval was ≥5 s.

iological properties and vice versa. For instance, Shaw2-P410A displayed the largest potentiation by 1-BuOH, but kinetics and voltage dependence of current activation did not seem different from Shaw2 wild-type, as shown before (Harris et al., 2003); the 1-BuOH sensitivity and voltage dependence of K_v2.1-P410A, K_v4.3-P400A and Shaw2 SK-P410A changed modestly relative to the wild-type counterparts, but current kinetics are dramatically affected (Figs. 5, 7–9). In contrast, however, the apparent voltage dependence and kinetics of K_v1.4-P557A, K_v3.4-P469A, K_v3.4 P469A-Shaw2 P410A, and K_v3.4 KS-P469A changed dramatically, and the potentiation by 1-BuOH was also significant but ~4- to ~1.5-fold smaller than that of Shaw2-P410A (Figs. 5–9). Finally, two hybrid K_v3.4-Shaw2 channels with PVAV mutations in the two distinct moieties displayed differential depolarizing shifts, but the corresponding 1-BuOH sensitivities seemed unchanged (Fig. 6 and 9). Therefore, these observations do not support a strict link between altered gating and sensitivity to 1-BuOH.

Discussion

Employing a combination of physiological, mutational, and structural analyses, we have investigated the putative concerted role of the S4–S5 linker and the S6-b segment on the functional modulation (inhibition and potentiation) of Shaw2 K^+ channel by 1-alkanols. The main results show that: 1) the α-helical propensity of the S4–S5 linker is a critical structural determinant of the modulation; 2) the magnitude of the potentiation depends on the number of PVAV mutations in a K_v channel tetramer; 3) a full complement of Shaw2 S4–S5 linkers and PVAV mutations in the K_v channel tetramer is necessary to support the maximum potentiation; 4) the PxAx mutation induces weak potentiation in mammalian K_v channels with divergent S4–S5 linkers; and 5) voltage-dependent activation and kinetics of K_v channels from different subfamilies depend critically on the presence of the second proline in the conserved PxPx motif in the S6 segment. The significance and possible implications of these findings are discussed below.

The Amphipathic S4–S5 Linker, a Structural Determinant of the Shaw2 1-Alkanol Site. The critical contribution of an amphipathic α-helical Shaw2 S4–S5 linker to 1-alkanol action is supported by several observations: 1) amphiphilic interactions are involved in the interactions between 1-alkanols and a site in the Shaw2 channel (Shahidullah et al., 2003); 2) relative to the K_v3.4 S4–S5 linker, the Shaw2 S4–S5 linker exhibits a higher α-helical propensity (Shahidullah et al., 2003); and 3) the Shaw2 S4–S5 linker confers inhibition by 1-alkanols in K_v3.4 channels, which are normally resistant to these agents (Harris et al., 2000). From the direct energetic correlation between the apparent 1-BuOH binding and the calculated α-helical propensity in the S4–S5 linkers of various mutants of the Shaw2 and K_v3.4 channels along with direct structural analyses (Figs. 2–4), we can conclude more firmly that the apparent higher affinity interaction between 1-alkanols and the Shaw2 channel depends on the higher α-helical stability in their S4–S5 linker. How would the S4–S5 secondary structure determine the 1-alkanol binding site? Structural studies showed that the S4–S5 linker of K_v channels (isolated or in the intact protein) adopts the α-helical structure, (Ohlenschlager et al., 2002; Long et al., 2005). Why, then, are most K_v channels resistant to 1-alkanols? An interesting possibility is that a relatively more stable α-helical structure in the Shaw2 S4–S5 linker would help to shape the putative protein-protein interface that constitutes the 1-alkanol site; furthermore, it would maintain the strong amphipathic character of the S4–S5 linker (Fig. 1), which is a critical feature of the Shaw2 1-alkanol site (Shahidullah et al., 2003). The presence of Ile319 near the middle of the Shaw2 S4–S5 linker (Fig. 1) may be particularly significant because glycine occupies the equivalent position in the majority of K_v channels that are resistant to 1-alkanols. Consistent with these ideas, the G371I mutation in K_v3.4 confers 1-alkanol sensitivity and increases the α-helical propensity of the S4–S5 linker (Covarrubias et al., 1995; Shahidullah et al., 2003). Glycine in the S4–S5 linker could introduce flexibility and possibly act as a hinge during gating of most K_v channels. This flexibility in the middle of the S4–S5 linker would contribute to a structural destabilization of the putative 1-alkanol site at the protein-protein interface.

PxPx: A Crucial Highly Conserved S6 Motif Involved in Gating and Modulation by 1-Alkanols in K_v Channels. Several studies have demonstrated the pivotal contribution of the PVPV motif in the S6-b region to voltage-dependent activation of Shaker and K_v1.5 channels (del Camino and Yellen, 2001; Hackos et al., 2002; Labro et al., 2003; Webster et al., 2004). Our data extend these studies to related mammalian K_v channels of different subfamilies and support their conclusions by demonstrating that PxAx mutations in K_v1.4, K_v2.1, K_v3.4, and K_v4.3 have a profound impact on voltage-dependent gating. That is to say, mutant channels exhibited slower activation and inactivation and a relative stabilization of the closed state (depolarized G_p-V relations). However, these effects were more dramatic on K_v1.4 and K_v3.4. If inactivation is coupled to activation and channel opening, an apparently slower current kinetics could result in part from more depolarized voltage-dependent activation. However, as proposed by other studies from our laboratory (Jerng et al., 1999), the elimination of inactivation in the K_v4.3-P400A mutant along with a modestly depolarized shift in the G_p-V relation indicates that a direct disruption of inactivation is also possible. The exact molecular mechanisms underlying the effects of PVAV mutations on gating are not well understood. It is possible that the loss of the second proline disrupts the S6 kink, which impairs a critical interaction between the S6-b segment and the S4–S5 linker and weakens the coupling with the voltage sensor. Therefore, the closed conformation of the activation gate is stabilized (in all K_v channels), and more specialized interactions responsible for inactivation gating are disrupted (in K_v4 channels). It is notable that the position corresponding to the second proline in the PxPx motif is replaced with other amino acids (Ala, Thr, Ser, or His) in electrically silent K_v subunits (K_v5, K_v6, and K_v8–K_v11) (Labro et al., 2003). Native substitutions at this critical location may contribute to the functional modulation of native heteromeric K_v channels by silent K_v subunits. It is therefore relevant that two PVAV mutations in a tetrameric K_v channel made of tandem heterodimers are sufficient to induce a relative stabilization of the closed state and confer potentiation by 1-BuOH and that the total number of PVAV substitutions in the tetramer determines the sensitivity (Figs. 6 and 9). Another important implication of

the tandem heterodimer results is that kinked and less kinked S6-b segments at the inner helix bundle of functional K_v tetramers are structurally compatible.

As described for the Shaw2 channel (Harris et al., 2003), the putative loss of the S6 kink at the second proline in the PxPx motif also conferred significant potentiation by 1-BuOH in two distinct mammalian channels, K_v1.4 and K_v3.4 (Fig. 7). In Shaw2 channels, 1-BuOH induces the potentiation by destabilizing the closed state of the channel (Harris et al., 2003), but the molecular basis of this modulation is still unknown. Nevertheless, the new observations show that the 1-BuOH potentiation conferred by the PxAx mutation is not restricted to the Shaw2 channel and that it results from a single substitution at a site that plays a critical functional role in eukaryotic K_v channels. Two apparent differences emerged from comparing the potentiation of Shaw2-P410A, K_v1.4-P557A and K_v3.4-P469A by 1-BuOH. First, in sharp contrast to K_v1.4-P557A and K_v3.4-P469A (Fig. 4–5), Shaw2-P410A does not induce an apparently more depolarized G_p-V relation (Harris et al., 2003); second, the potentiation of Shaw2-P410A is 4- to 5-fold larger than that of the other two mutants (Fig. 7). A more depolarized voltage-dependent activation of Shaw2-P410A channels may not be detected because the open probability and voltage dependence of these channels is intrinsically very low (Tsunoda and Salkoff, 1995; Smith-Maxwell et al., 1998). In general, one could then argue that the PxAx mutation induces a relative stabilization of a closed state, which allows the allosteric 1-BuOH potentiation by creating a favorable conformation. However, an allosteric mechanism that simply associates modulation by 1-alkanols to the relative stabilities of the closed or open states (i.e., the voltage dependence of the G_p-V curves) is not supported generally by the data (Figs. 5–9). The structural perturbation caused by the PxAx mutation could also change the 1-alkanol site in the interface between the S4–S5 linker and the S6-b segment. Such a local change may then determine the potentiation by 1-alkanols. Other results discussed below favor this possibility.

The 1-Alkanol Site in the Amphipathic Interface between S4–S5 and S6-B in the Shaw2 Channel. Swapping of the S4–S5 linkers between Shaw2-P410A and K_v3.4-P469A showed that the S4–S5 linker of K_v3.4 suppresses the potentiation by 1-BuOH and that of Shaw2 enhances it (Fig. 5). Therefore, as for the inhibition by 1-alkanols, the magnitude of the potentiation by 1-BuOH also depends significantly on the structure of the S4–S5 linker. Although the enhanced potentiation of K_v3.4-KS P469A was associated with a depolarized shift in the voltage dependence of current activation (relative to K_v3.4-P469A), the suppressed potentiation of Shaw2-SK P410A was not associated with an opposite shift (relative to Shaw2-P410A) (Fig. 9D). It is possible that binding to a site involving the S4–S5 linker may also underlie the potentiation of K_v channels by 1-BuOH. We propose that the amphipathic S4–S5 linker and a mostly hydrophobic S6-b segment below the PxPx motif may together shape a protein-protein interface that constitutes the 1-alkanol site. The presence or absence of the α-helix kink at the S6 PxPx motif determines whether binding of 1-alkanols to this site stabilizes (inhibition) or destabilizes (potentiation) the closed state of the Shaw2 channel.

Inspection of the K_v1.2 crystal structure and computational structural models of K_v channels (Durell et al., 2004; Long et al., 2005) revealed that the interface between the S4–S5 linker and the S6-b segment exhibits the amphipathic character and the molecular features predicted by the known structure of a 1-alkanol site in the *D. melanogaster* LUSH protein cocrystallized with ethanol and 1-BuOH (Kruse et al., 2003). The amphipathic LUSH 1-alkanol site is located in the interface between two α-helical segments (α3 and α6). In this interface, hydrophobic (aromatic) and polar residues (Thr and Ser) interact with a single 1-alkanol molecule. These polar residues are part of an H-bond network that stabilizes the 1-alkanol in the site. Based on this similarity, we have proposed a docking model of 1-butanol in the interface between the S4–S5 linker and the S6-b segment of the Shaw2 channel in the closed state (Covarrubias et al., 2005). It would seem, as demonstrated in the LUSH protein (Kruse et al., 2003), that the bound 1-alkanol molecule stabilizes the structure of the interface in the resting state of the Shaw2 channel to cause inhibition (Harris et al., 2003). By analogy, one could speculate that the relative destabilization of the resting state upon 1-alkanol binding (potentiation) may result from stabilizing the interface in a configuration that favors the activated preopen state of the channel with a disrupted S6 kink.

Acknowledgments

We thank the Covarrubias lab and Dr. Richard Horn for fruitful discussions and suggestions, and Nathan Klett for testing volatile anesthetics on Shaw2 channels. In addition, we thank Dr. Yuri Kaulin (Thomas Jefferson University), Dr. Spencer Yost (UC San Francisco), and Dr. David Jones (University of Colorado, Denver, CO) for their critical reading of the manuscript.

References

Anantharam V, Bayley H, Wilson A, and Treistman SN (1992) Differential effects of ethanol on electrical properties of various potassium channels expressed in oocytes. *Mol Pharmacol* **42:**499–505.
Beck EJ and Covarrubias M (2001) K_v4 channels exhibit modulation of closed-state inactivation in inside-out patches. *Biophys J* **81:**867–883.
Campagna JA, Miller KW, and Forman SA (2003) Mechanisms of actions of inhaled anesthetics. *N Engl J Med* **348:**2110–2124.
Cantor CR and Schimmel PR (1980) *Biophysical Chemistry: Part III The Behavior of Biological Macromolecules,* W.H. Freeman and Company, San Francisco, CA.
Covarrubias M, Bhattacharji A, Harris T, Kaplan B, and Germann MW (2005) Alcohol and anesthetic action at the gate of a voltage-dependent K^+ channel, in *Basic and Systemic Mechanisms of Anesthesia* (Mashimo T, Ogli K, and Uchida I eds) pp 55–60, Elsevier B.V., Amsterdam.
Covarrubias M, Vyas TB, Escobar L, and Wei A (1995) Alcohols inhibit a cloned potassium channel at a discrete saturable site. Insights into the molecular basis of general anesthesia. *J Biol Chem* **270:**19408–19416.
Covarrubias M, Wei A, Salkoff L, and Vyas TB (1994) Elimination of rapid potassium channel inactivation by phosphorylation of the inactivation gate. *Neuron* **13:**1403–1412.
del Camino D and Yellen G (2001) Tight steric closure at the intracellular activation gate of a voltage-gated K^+ channel. *Neuron* **32:**649–656.
Diamond I and Gordon AS (1997) Cellular and molecular neuroscience of alcoholism. *Physiol Rev* **77:**1–20.
Ding S and Horn R (2003) Effect of S6 tail mutations on charge movement in shaker potassium channels. *Biophys J* **84:**295–305.
Durell SR, Shrivastava IH, and Guy HR (2004) Models of the structure and voltage-gating mechanism of the shaker K^+ channel. *Biophys J* **87:**2116–2130.
Ferrer T, Rupp J, Piper DR, and Tristani-Firouzi M (2006) The S4–S5 linker directly couples voltage sensor movement to the activation gate in the HERG K^+ channel. *J Biol Chem* **281:**12858–12864.
Hackos DH, Chang TH, and Swartz KJ (2002) Scanning the intracellular s6 activation gate in the shaker K^+ channel. *J Gen Physiol* **119:**521–532.
Harris RA (1999) Ethanol actions on multiple ion channels: which are important? *Alcohol Clin Exp Res* **23:**1563–1570.
Harris T, Graber AR, and Covarrubias M (2003) Allosteric modulation of a neuronal K^+ channel by 1-alkanols is linked to a key residue in the activation gate. *Am J Physiol* **285:**C788–C796.
Harris T, Shahidullah M, Ellingson JS, and Covarrubias M (2000) General anesthetic action at an internal protein site involving the S4–S5 cytoplasmic loop of a neuronal K^+ channel. *J Biol Chem* **275:**4928–4936.
Hemmings HC Jr, Akabas MH, Goldstein PA, Trudell JR, Orser BA, and Harrison NL (2005) Emerging molecular mechanisms of general anesthetic action. *Trends Pharmacol Sci* **26:**503–510.

Hodge JJ, Choi JC, O'Kane CJ, and Griffith LC (2005) Shaw potassium channel genes in *Drosophila*. *J Neurobiol* **63:**235–254.
Jerng HH, Shahidullah M, and Covarrubias M (1999) Inactivation gating of K_v4 potassium channels: molecular interactions involving the inner vestibule of the pore. *J Gen Physiology* **113:**641–660.
Kruse SW, Zhao R, Smith DP, and Jones DN (2003) Structure of a specific alcohol-binding site defined by the odorant binding protein LUSH from *Drosophila melanogaster*. *Nat Struct Biol* **10:**694–700.
Labro AJ, Raes AL, Bellens I, Ottschytsch N, and Snyders DJ (2003) Gating of shaker-type channels requires the flexibility of S6 caused by prolines. *J Biol Chem* **278:**50724–50731.
Lacroix E, Viguera AR, and Serrano L (1998) Elucidating the folding problem of alpha-helices: local motifs, long-range electrostatics, ionic-strength dependence and prediction of NMR parameters. *J Mol Biol* **284:**173–191.
Long SB, Campbell EB, and MacKinnon R (2005) Voltage sensor of $K_v1.2$: structural basis of electromechanical coupling. *Science (Wash DC)* **309:**903–908.
Lu Z, Klem AM, and Ramu Y (2002) Coupling between voltage sensors and activation gate in voltage-gated K^+ channels. *J Gen Physiol* **120:**663–676.
Muñoz V and Serrano L (1994) Elucidating the folding problem of helical peptides using empirical parameters. *Nat Struct Biol* **1:**399–409.
Ohlenschlager O, Hojo H, Ramachandran R, Gorlach M, and Haris PI (2002) Three-dimensional structure of the S4–S5 segment of the shaker potassium channel. *Biophys J* **82:**2995–3002.
Peoples RW, Li C, and Weight FF (1996) Lipid vs protein theories of alcohol action in the nervous system. *Annu Rev Pharmacol Toxicol* **36:**185–201.
Rettig J, Wunder F, Stocker M, Lichtinghagen R, Mastiaux F, Beckh S, Kues W, Pedarzani P, Schroter KH, Ruppersberg JP, et al. (1992) Characterization of a shaw-related potassium channel family in rat brain. *EMBO (Eur Mol Biol Organ) J* **11:**2473–2486.
Salkoff L, Baker K, Butler A, Covarrubias M, Pak MD, and Wei A (1992) An essential 'set' of K^+ channels conserved in flies, mice and humans. *Trends Neurosci* **15:**161–166.
Shahidullah M, Harris T, Germann MW, and Covarrubias M (2003) Molecular features of an alcohol binding site in a neuronal potassium channel. *Biochemistry* **42:**11243–11252.
Smith-Maxwell CJ, Ledwell JL, and Aldrich RW (1998) Role of the S4 in cooperativity of voltage-dependent potassium channel activation. *J Gen Physiol* **111:**399–420.
Sreerama N, Venyaminov SY, and Woody RW (2000) Estimation of protein secondary structure from circular dichroism spectra: inclusion of denatured proteins with native proteins in the analysis. *Anal Biochem* **287:**243–251.
Sreerama N and Woody RW (2000) Estimation of protein secondary structure from circular dichroism spectra: comparison of CONTIN, SELCON, and CDSSTR methods with an expanded reference set. *Anal Biochem* **287:**252–260.
Sreerama N and Woody RW (2004) On the analysis of membrane protein circular dichroism spectra. *Protein Sci* **13:**100–112.
Tristani-Firouzi M, Chen J, and Sanguinetti MC (2002) Interactions between S4–S5 Linker and S6 transmembrane domain modulate gating of HERG K^+ channels. *J Biol Chem* **277:**18994–19000.
Tsunoda S and Salkoff L (1995) Genetic analysis of *Drosophila* neurons: Shal, Shaw, and Shab encode most embryonic potassium currents. *J Neurosci* **15:**1741–1754.
Webster SM, Del Camino D, Dekker JP, and Yellen G (2004) Intracellular gate opening in shaker K^+ channels defined by high-affinity metal bridges. *Nature (Lond)* **428:**864–868.
Wüthrich K (1986) *NMR of Proteins and Nucleic Acids.* Wiley-Interscience, New York.
Yifrach O and MacKinnon R (2002) Energetics of pore opening in a voltage-gated K^+ channel. *Cell* **111:**231–239.

Address correspondence to: Manuel Covarrubias, Department of Pathology, Anatomy and Cell Biology, Jefferson Medical College of Thomas Jefferson University, 1020 Locust Street, Philadelphia, PA 19107. E-mail: manuel.covarrubias@jefferson.edu